Nonadiabatic ab initio Molecular Dynamics of Photoisomerization Reaction between 1,3-Cyclohexadiene and 1,3,5-cis-Hexatriene

ARTICLE *in* CHEMICAL PHYSICS · JULY 2015

Impact Factor: 1.65 · DOI: 10.1016/j.chemphys.2015.07.024

4 AUTHORS, INCLUDING:

Sebastian O Danielache

Sophia University

28 PUBLICATIONS **259** CITATIONS

SEE PROFILE

Shinkoh Nanbu

Sophia University

107 PUBLICATIONS **897** CITATIONS

SEE PROFILE

Chemical Physics 459 (2015) 45–53

Contents lists available at ScienceDirect

Chemical Physics

journal homepage: www.elsevier.com/locate/chemphys

Nonadiabatic *ab initio* molecular dynamics of photoisomerization reaction between 1,3-cyclohexadiene and 1,3,5-*cis*-hexatriene

Ayumi Ohta, Osamu Kobayashi, Sebastian O. Danielache, Shinkoh Nanbu *

Department of Material and Life Sciences, Faculty of Science & Technology, Sophia University, 7-1 Kioi-Cho, Chiyoda-Ku, Tokyo 102-8554, Japan

ARTICLE INFO

Article history:
Received 15 May 2015
In final form 20 July 2015
Available online 30 July 2015

Keywords:
Ab initio molecular dynamics
Nonadiabatic transition
Photochromic molecule
Excited states dynamics
Zhu–Nakamura version trajectory surface hopping

ABSTRACT

The photoisomerization process between 1,3-cyclohexadiene (CHD) and 1,3,5-*cis*-hexatriene (HT) has been studied by nonadiabatic *ab initio* molecular dynamics based on trajectory surface-hopping approach with a full-dimensional reaction model. The quantum chemical calculations were treated at MS-MR-CASPT2 level for 8 electrons in 8 orbitals with the cc-pVDZ basis set. The Zhu–Nakamura formula was employed to evaluate nonadiabatic transition probabilities. S_1 and S_2 states were included in the photoisomerization dynamics. Lifetimes and CHD:HT branching ratios were computationally estimated on the basis of statistical analysis of multiple executed trajectories. The analysis of trajectories suggested that the nonadiabatic transitions at the S_0/S_1 and S_1/S_2 conical intersections (CoIn) are correlated to the Kekulé-type vibration and the C3–C4–C5 bending motion, respectively. The one-sided branching ratio was obtained by excitations to the S_2 state; 70:30. The critical branching process was found to be dominated by the location of CoIn in potential energy hypersurface of the excited state.

1. Introduction

Photoinduced ring opening/closure of photochromic molecules such as diarylethenes and fulgides has been frequently applied to molecular switches and memories [1–4]. The application of molecular switch as propelled by the study of ultrafast photochemical systems promotes better understanding the mechanism of short lived photochromic systems which allows us to extract the product branching ratio. The photoisomerization between 1,3-cyclohexadiene (CHD) and 1,3,5-*cis*-hexatriene (HT) is the fascinated reaction centered in diarylethenes; the photochromism is originally derived from the photoisomerization of CHD/HT (see Fig. 1). This prototype photoreaction has attracted a great deal of interest as a simple model system in both theoretical [5–19] and experimental [20–39] studies. Kosma et al. have experimentally observed the CHD/HT isomerization with time-resolved photoelectron/mass spectroscopy [37]. CHD was photoexcited to S_1 by the ultrashort third harmonic pulse (270 nm). They reported that molecular wavepacket passes through the conical intersection (CoIn) of $1^1B/2^1A$ (S_1/S_2) at about 56 fs after photoexcitation, and then the wavepacket is deactivated into S_0 through the CoIn of $2^1A/1^1A$ (S_0/S_1) at approximate 136 fs.

On the other hand, Tamura et al. studied quantum dynamics of this reaction by using the wavepacket propagation method on a two-dimensional potential energy surface [16]. The branching ratio between CHD and HT was found to be 50:50 in their model. In addition the time duration of the first decay $1^1B–2^1A$ is approximately 15–25 fs, and then molecular wavepacket gets through next CoIn of S_0/S_1 at 130 fs. Other discussions about the experimental CHD:HT ratio in cyclohexane have been reported as 60:40 in solution [27]. Hofmann and de Vivie-Riedle also performed the wavepacket dynamics using the effective Hamiltonian based on the two dimensional model [12]. The correlation between theoretical CHD:HT ratios and locations of CoIn was discussed in their report. Many other theoretical studies have been also reported so far. But the simulation has not been yet carried out to treat all degrees of freedom; the effective Hamiltonian has been employed to reduce computational cost. In those discussions, the two-dimensional model has been used widely; i.e. the two coordinates consist of the ring opening degree of CHD and the dihedral angle. This coordinate-restriction ignores the other vibrational modes and their anharmonicity aside from those included in the two dimensions and it also reduces the phase space in molecular dynamics. The small volume of phase space might produce a wrong insight. In the present work, the photoisomerization in the full-dimensional model (42 degrees of freedom) was explored by nonadiabatic molecular dynamics based on Zhu–Nakamura formula and trajectory surface-hopping (TSH) approach.

Prior to photoexitation, the most stable structure of a molecule resides in the bottom of the electronic ground state well. After

* Corresponding author.
E-mail address: shinkoh.nanbu@sophia.ac.jp (S. Nanbu).

http://dx.doi.org/10.1016/j.chemphys.2015.07.024
0301-0104/

photoexitation, a re-conformation of the chemical bonds takes place and C_2 symmetry can no longer be assumed. Numerous theoretical studies of this reaction assumed a fixed C_2 symmetry during the photoisomerization process. This assumption was quite reasonable to reduce the computational cost, but it ignores any conformational change of the molecule after photoexcitation. Forbidden transitions turn into allowed transitions when a very important property associated to the change of symmetry occurs. For example, the vertical excitation to the first excited state of sulfur carbonyl (OCS) molecule is forbidden in the linear configuration (C_{2v} symmetry), but it becomes an allowed transition once the molecule is slightly bending. The OCS actually shows a strong broad photoabsorption cross section due to S_1 excitation in C_s symmetry [40,41]. The broad UV absorption spectrum of CHD has been already reported in Ref. [37] as assigned to the 2^1A (S_2) transition. In the present work, the *ab initio* molecular dynamics (AI-MD) are performed by the excitation to S_2 as well as S_1.

A complex mixing of several electronic structures hides behind the superficial molecular structure-deforming in this reaction-mechanism. In order to account for the change in conformational structure, it is necessary to employ on-the-fly AI-MD which provides a solution for nuclear motions during the process of this isomerization. There are a number of approaches that combines a classical MD while considering state-transitions; these are TSH method [42], and the "fewest switches" TSH method [43]. We adopted the ZN-TSH method [44–49] in the present work. ZN-TSH formula is the powerful tool to analyze nonadiabatic transition probability between some electric states [50–59]. In particular, Zhu–Nakamura theory allows us to solve the over-coherence problem and to treat non-vertical hops [60,61]. The ZN-TSH theory helps us to get more accurate insight for the mechanisms of nonadiabatic process with the minimum computational effort.

2. Methodology

2.1. Ab initio MO MRCI/CASPT2 calculations

State-averaged complete active space self-consistent field (SA-CASSCF) method was employed to determine molecular orbitals (MOs). And then, multi-reference configuration interaction (MRCI) and multi-state multi-reference complete active space second perturbation theory (MS-MR-CASPT2) calculations were performed by using correlation-consistent polarized-valence double-ζ (cc-pVDZ) basis functions [62]. The main electronic configuration of the S_0 state of CHD is written as (inner occupied orbitals)^{36} $(19a)^2$ $(20a)^2$ $(21a)^2$ $(22a)^2$ $(23a)^0$ $(24a)^0$ $(25a)^0$ $(26a)^0$ in C_1 symmetry. Fig. 2 illustrates MOs, (19*a*)–(26*a*). Since this photoisomerization involves the ring opening/closure reaction, π-bond breaking and regenerating are important. As shown in Fig. 2, (22*a*) and (24*a*) assigned to π and π^* are characterized with C2–C3 π + C4–C5 π bonding and its anti-bonding orbitals, which are a kind of paired orbitals for the active space to describe the bond formation and cleavage. This pair is important for performing the MD simulation. In this sense, (20*a*) and (25*a*) are also paired π orbitals, while (21*a*) and (23*a*) are assigned to the paired σ and σ^* orbitals. These paired orbitals are significant to describe the bond nature for C1–C6 bond. On the other hand, orbital energies of (19*a*) and (26*a*) were found to be lying closely to (20*a*) and (25*a*), respectively. The (19*a*) and (26*a*) orbitals moreover indicates the other σ and σ^* paired orbitals as seen in Fig. 2. In terms of the reforming π-bond and the orbital energies of each MO, eight MOs (19*a*)–(26*a*) were significant. The valance space occupied by eight electrons was constructed with these eight MOs, which were also assigned as the active space (8e,8o) in the way that can be described like

$$[(19a)(20a)(21a)(22a)(23a)(24a)(25a)(26a)]^8.$$

At the MRCI calculation, Davidson correction was included to account for contributions of quadruple excitations to the correlation energy. All of the *ab initio* calculations were carried out using the electronic structure program Molpro 2012.1 [63].

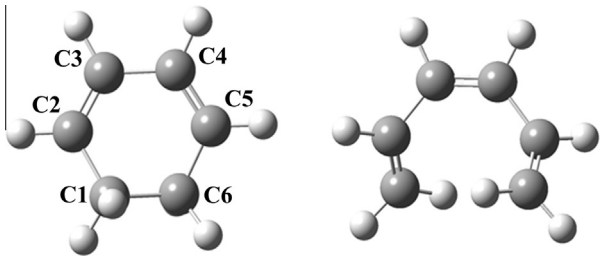

Fig. 1. 1,3-cyclohexadiene (left) and 1,3,5-*cis*-hexatriene (right).

2.2. Nonadiabatic molecular dynamics

On-the-fly *ab initio* molecular dynamics (AI-MD) were executed out in which nonadiabatic transitions were taken into account. The same procedure for electronic part of the AI-MD simulations was used as mentioned in the *ab initio* calculations; MS-MR-CASPT2 method with cc-pVDZ was performed to compute the potential energies and its gradients of three electronic states, S_0, S_1, and S_2. Table 1 lists vertical excitation energies, transition dipole moments (TDM) and CPU times calculated by CASPT2 method with the equilibrium geometry in S_0 using various basis sets. In addition, Table 2 shows the vertical excitation energies by CASPT2 and MRCI methods to make sure of the accuracy of the calculation method for the AI-MD with comparing the experimental data. The verification of the rationale of our theoretical approach is discussed in Section 3.

The classical trajectories for nuclear motions were evolved with time by velocity Verlet algorism [64]. The time step was 0.25 fs, and the trajectories were propagated until the isomerization is completed. The initial molecular coordinates and momenta were generated using random numbers subject to the Wigner distribution [65]; the distribution reflects vibrational wave functions at the zero-point energy (ZPE) level, which was computed with the use of the analytical Hessian matrix obtained by the CASSCF calculation for the electronic ground state.

The trajectory surface-hopping procedure is based on the Zhu–Nakamura theory, which provides a complete set of solutions for potential energy curve-crossing problems over the whole energy range. The multidimensional ZN-TSH scheme has been successfully applied to a number of systems [66–69]. The procedure is summarized as follows; the nonadiabatic coupling vector is calculated when the energy difference between the two adjacent adiabatic potential energy surfaces is a local minimum, and then the one-dimensional adiabatic potential curves are calculated in the direction of the coupling vector and the transition probability for this one-dimensional curve crossing is calculated using analytical formulas of the Zhu–Nakamura theory. The nonadiabatic coupling vectors were determined at the SA-CASSCF level. The decision whether the transition to the adjoining potential energy surface (PES) occurs or the trajectory stays on the same PES is made by using an anteater method [42]. The parameters of the trajectory after hop are reconfigured so that the total energy of the trajectory is conserved. When the kinetic energy is not enough for the vertical hop, the transition becomes non-vertical with the energy conservation. Non-vertical hop corresponds to a classically forbidden transition due to tunneling. The classically allowed transitions at

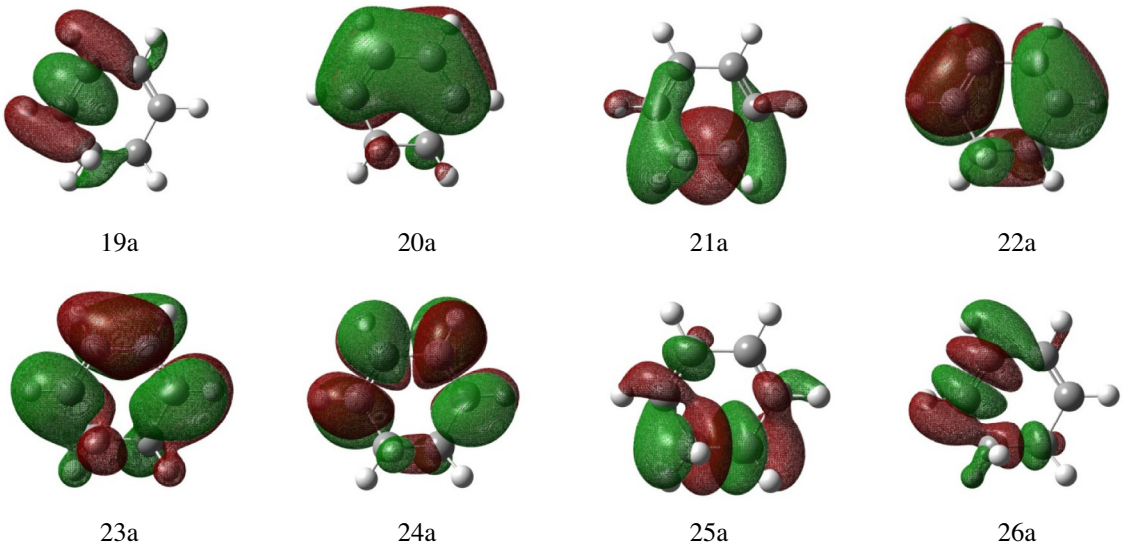

Fig. 2. Molecular orbitals belonging to the active space.

Table 1
Vertical excitation energies, transition dipole moments and CPU time calculated by CASPT2 with the equilibrium geometry in S_0 using various basis sets.

Basis set	Excitation energy/eV		TDM/Debye		Computational cost/sandybridge core
	$S_1 \leftarrow S_0$	$S_2 \leftarrow S_0$	$S_1 \leftarrow S_0$	$S_2 \leftarrow S_0$	CPU time/s
cc-pVDZ	5.51	6.34	0.21	2.59	32,789
aug-cc-pVDZ	5.31	5.97	0.34	1.26	265,927
cc-pVTZ	5.38	6.50	0.26	2.64	164,722

Table 3
Transition dipole moments (TDM) at MRCI levels with different symmetries.

MRCI (our initial coordinate[a])/ Debye		MRCI (C_2)/Debye	
Transition pattern	TDM	Transition pattern	TDM
$S_1 \leftarrow S_0$	0.63	$1^1B \leftarrow 1^1A$ ($S_1 \leftarrow S_0$)	2.73
$S_2 \leftarrow S_0$	2.65	$2^1A \leftarrow 1^1A$ ($S_2 \leftarrow S_0$)	0.28

[a] See text for detailed discussion.

the energies near the crossing point can be also treated accurately in the present scheme.

All of our AI-MD simulations were performed on Intel XEON (Westmere, Nehalem, and Sandybridge cores) computers (TS3DR2, CONCURRENT SYSTEMS Ltd.). Totally eighty-seven trajectory-computations were executed and it took eleven months to compute all of these calculations using these computers.

3. Results and discussion

Transition dipole moments (TDM) were explored by MRCI method at the equilibrium geometry of S_0. Table 3 shows the dependence analysis for TDM for C_2 symmetry/asymmetry on the electronic structure calculations. The asymmetric structures here were one of our initial coordinates reflecting the zero-point vibration mentioned in Section 2. Especially when C_2 symmetry have been broken, the TDM for the excitation to the S_2 state have a certain amount. Thus, the excitation to S_2 was explored to understand the photoisomerization mechanism.

As mentioned in Section 2, Table 1 lists the results obtained by CASPT2 method with the equilibrium geometry in S_0 using various basis sets, i.e. the vertical excitation energy, TDM and the CPU time. The CPU time at cc-pVTZ level was at least 5 times as long as that at cc-pVDZ. As to the computation at the aug-cc-pVDZ level, it took much longer than the level of cc-pVTZ. In terms of the excitation energy, there was not much of a distinction in the appearance between each results. To obtain a more representative result for statistical analysis, we finally traded off a larger basis set for a larger number of trajectories. Thus, the cc-pVDZ basis sets would be reasonable for the AI-MD simulation.

Table 2
Excitation energy at CASPT2 and MRCI levels.

Excitation energy/eV				
Electronic state	CASPT2	MRCI	MRCI (C_2)	Experiment[a]
S_0	0	0	0	0
S_1	5.51	5.62	5.77	4.59
S_2	6.34	6.42	6.64	5.55

[a] Estimated by experimental data in Ref. [37].

Furthermore, the vertical excitation energy by MRCI method has moreover been computed to make sure of the vertical excitation energies evaluated from CASPT2 calculations, because the CASPT2 method has a strong trend of energy-stabilization only for ionic state as reported by Gozem et al. [70]. The results computed by MRCI method with C_1 and C_2 symmetries are listed in Table 2 with experimental data [37]. Since the results by CASPT2 and MRCI methods are quite similar to each other, the CASPT2 method was a reasonable method to simulate this photoisomerization accurately with a smaller amount of computational cost. We have however apprehended that there is some energy-differences between experimental value and theoretical data; our theoretical data seem to be higher than the experimental data by approximately 1 eV. The two assumable reasons for this energy difference would be explained by our theoretical approach and experimental evidence.

In our theoretical approach, the CAS space was composed of CAS(8e,8o), but the reference space generated by CAS(8e,8o) for MRCI and CASPT2 would not be enough to describe the electronic structures of S_1 and S_2. Note that the level of the basis sets does not strongly affect the vertical excitation energies. In contrast, there is the fact that the smaller active space calculation at CAS(6e,6o)SCF/6-31G* level [8] has provided us the similar

excitation energies to our results by CASPT2 and MRCI based on CAS(8e,8o)SCF. Therefore, the vertical excitation energies would not be improved dramatically, even if we performed a larger active space like CAS(16e,16o) for MRCI and CASPT2.

From the experimental point of view, the broadband spectrum implies that the photoexcitation is due to the bound-free transition, because Kosma et al. have observed the broad UV photoabsorption spectrum [37]. The bound-free transition happens with the strong conformational change like the linear-bent transitions of carbonyl sulfide (OCS) and nitrous oxide (N_2O) [71,72]. In both cases, the theoretical result differed from the experimental data by about 1 eV, compared with the vertical excitation energy obtained by MRCI methods at the equilibrium geometry. This situation would happen in the CHD system.

The primary electronic configuration of the S_1 state of CHD features mixed excitations of $(22a)^2 \rightarrow (23a)^2$ and $(21a)^1 \rightarrow (23a)^1$; their reference coefficients are 0.619 and 0.492, respectively. The primary electronic configuration of S_2 is a single excitation of $(22a)^1 \rightarrow (23a)^1$. Fig. 2 shows MOs belonging to the active space. This suggests that both of excitations to S_1 and S_2 conduce to π-bond breaking and reformation of double bonds. Thus, these two excitations could indicate CHD to make a structural change.

3.1. Time-profile of potential energies and molecular structures

The forty-two trajectories were prepared for our AI-MD simulations excited to S_1. Fig. 3 shows time-evolution of potential energies for a typical trajectory. The solid and dash lines represent a current electronic state and nearby empty states. The S_0, S_1 and S_2 states are drawn by the blue, green and red lines. As shown in Fig. 3, the fluctuation of energy was present along with time-evolution of molecular structures and electronic states. The nonadiabatic transition happens at 66.25 fs, and then the trajectory returns to the electronic ground state in a typical trajectory shown in Fig. 3. Fig. 4 shows time-profile of all potential energies of the propagated trajectories after excitation to S_1; S_0 (blue) and S_1 (green) appear with rare events of the transition to S_2.

The forty-five trajectories were also propagated after excitations to S_2. Time-evolution of potential energy along a typical trajectory is shown in Fig. 5. The first nonadiabatic transition between S_2 and S_1 happens at 19.75 fs, and the second nonadiabatic transition between S_1 and S_0 occurs at 48.5 fs in Fig. 5. Fig. 6 shows time-profile of all potential energies along all trajectories. The first decay

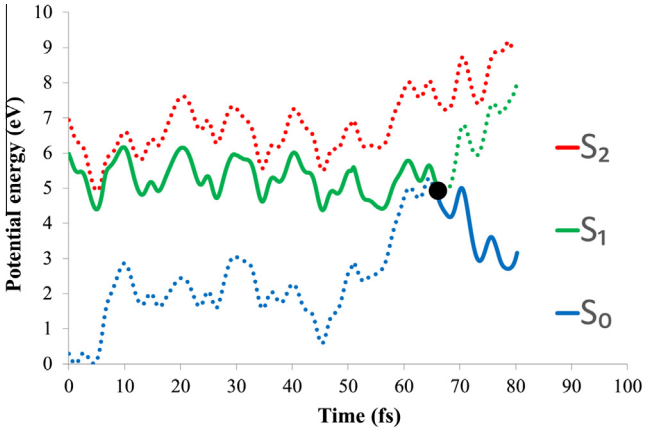

Fig. 3. Time-evolution of potential energies along the typical trajectory after photoexcitation to S_1; the time when the nonadiabatic transition happened corresponds to the black circle and changing a line-color. (For interpretation of the references to color in this figure legend, the reader is referred to the web version of this article.)

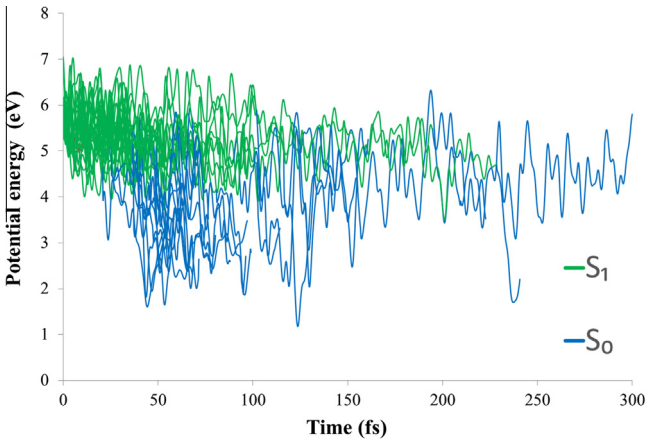

Fig. 4. Time-evolution of potential energies of all propagated trajectories in photoexcitation to S_1; the time when the nonadiabatic transition happened corresponds to changing a line-color. (For interpretation of the references to color in this figure legend, the reader is referred to the web version of this article.)

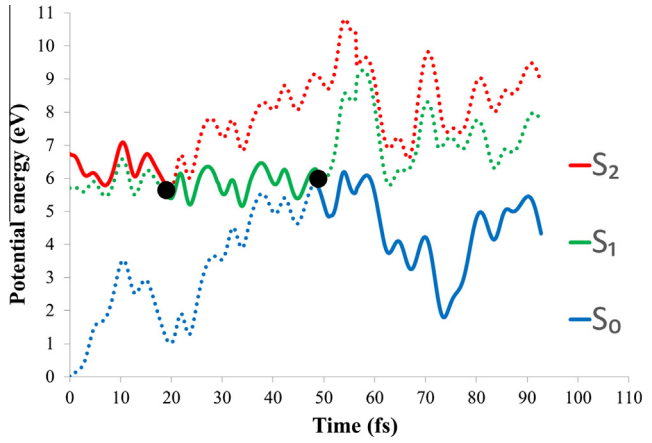

Fig. 5. Time-evolution of potential energies along the typical trajectory after photoexcitation to S_2; the time when the nonadiabatic transition happened corresponds to the black circle and changing a line-color. (For interpretation of the references to color in this figure legend, the reader is referred to the web version of this article.)

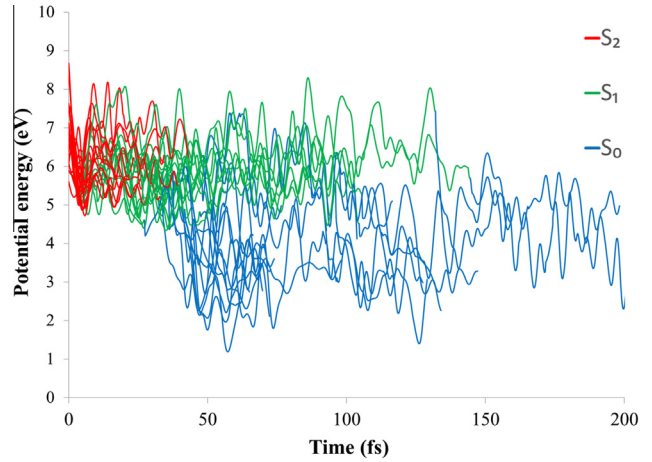

Fig. 6. Time-evolution of potential energies of all propagated trajectories in photoexcitation to S_2; the time when the nonadiabatic transition happened corresponds to changing a line-color. (For interpretation of the references to color in this figure legend, the reader is referred to the web version of this article.)

times between S_2 and S_1 were found to be shorter than the second decay.

Fig. 7 shows the time-evolution of the C1–C6 bond length in the photoexcitation to S_1. As shown before, each color indicates the state that the trajectory runs on; the respective S_1 and S_0 states were plotted by the green and blue lines. The time when nonadiabatic transitions happened corresponds to changing a line-color. The C1 and C6 atoms play a significant role in bond-reconstruction of the photochromic mechanism between CHD and HT. The C1–C6 bond length of the most stable CHD is 1.56 Å in S_0, while the length of the HT is 3.46 Å. But there were some trajectories that indicated the longer bond length than 3 Å, which suggested that the isomerization to other structural isomers of HT i.e. cZt-HT and tZt-HT happened. In gas phase, intramolecular energy redistribution occurs, then the redistribution leads to structural deforming steadily. The ring-opening of CHD started at an early stage around 50 fs before the nonadiabatic transitions occurred (68 fs) shown in Table 4.

3.2. Excited state lifetimes and decay processes

In order to produce a parameter that can be contrasted to experimental data, the lifetime of the photoisomerization process was calculated. Each classical trajectory has its own lifetime depending on the time when nonadiabatic transition happens after photoexcitation in its MD simulation, and the final result is defined by the accumulation analysis of all computed trajectories. In the present work, the population analysis of the electronic states was performed to obtain the lifetime with the accumulated data.

Fig. 8 shows the time evolution of the fraction of trajectories in S_1 after excitation to S_1. A single exponential function curve fit was the optimum method to describe the population decay process. The total lifetime ($t_{state,total}$) of a certain excited state is given by fitting the time-profile of the fraction of trajectories to the single exponential function:

$$t_{state,total} = t_{lat} + t_{dec} \tag{1.1}$$

$$P(t) = \exp\left(-\frac{t - t_{lat}}{t_{dec}}\right) \tag{1.2}$$

where t_{lat} and t_{dec} are latency and decay constants. $P(t)$ is the fitting single exponential function. The latency time describes the time taken from the photoexcitation to the first decay. In other words, t_{lat} means the time all trajectories stay in each excited state, which is illustrated in Figs. 8 and 11. The total lifetime of each excited state ($t_{state,total}$) is defined by the sum of t_{lat} and t_{dec}.

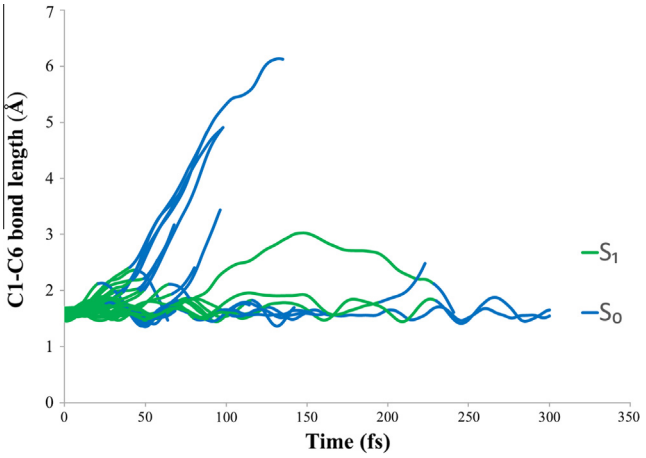

Fig. 7. Time-evolution of the C1–C6 bond after photoexcitation to S_1; the time when the nonadiabatic transition happened corresponds to changing a line-color. (For interpretation of the references to color in this figure legend, the reader is referred to the web version of this article.)

Table 4
Time constants determined by fitting to exponential functions.

	Excitation to S_1 ($t_{S_1,total}$)	Excitation to S_2 ($t_{S_2,total}$)
t_{lat}	21	4
t_{dec}	47	19
Total	68 fs	23 fs

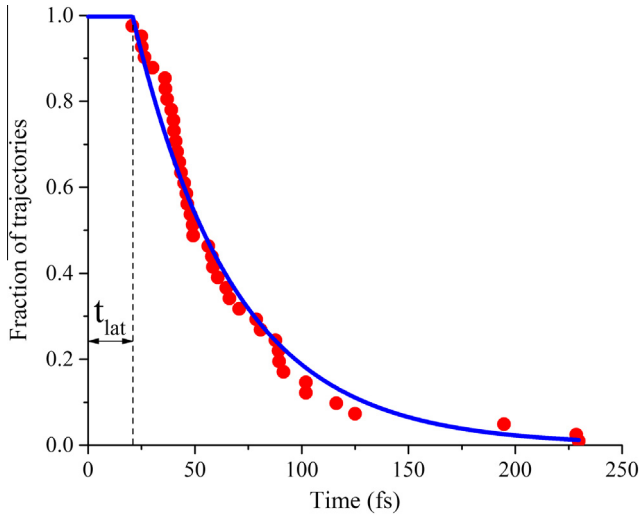

Fig. 8. Fraction of trajectories in S_1 after photoexcitation to S_1; red points were given by our simulations, while the blue line was the decay curve determined by Eq. (1.2). (For interpretation of the references to color in this figure legend, the reader is referred to the web version of this article.)

All optimized constants are listed in Table 4; Fig. 8 shows the obtained $P(t)$ for S_1 excitation drawn by the blue line, compared to the red sample points. Then the total lifetime of S_1 ($t_{S_1,total}$) was found to be 68 fs. This theoretical lifetime would be shorter than experimental data (136 fs) [37], our results would however agree with the data at the scale of femtoseconds. It should be noted that our simulations correspond to the photoexcitation by flash lamp irradiation with the broad band spectrum. In other words, the different initial conditions from the experimental setup using the laser excitation were used to simulate the photoisomerization in the present work.

On the other hand, meaningful deviations of our sample data (red points) was clearly seen from the $P(t)$ (blue line), which is shown in Fig. 9. Kosma et al. measured the quantum beat using coherent oscillations, and assigned to some vibrations. The fast Fourier transform (FFT) would be the ideal way to look at the major periodic motions approaching the nonadiabatic transition points, and the motions would be correlated with the vibrational motions at the conical intersections. Therefore, FFT was also performed for our deviations, which is shown in Fig. 10. Three big peaks appeared at 260, 350, and 440 cm^{-1}, and two small peaks also appeared at 750 and 910 cm^{-1}. In addition to the FFT analysis, the vibration frequency analysis was performed with using the molecular geometry extracted at the trajectory running near CoIn on S_1 with CASPT2/cc-pVDZ level. Then the assignment of these frequencies have been carried out by comparing with vibrational modes given by the vibration frequency analysis and these results are shown in Table 5. The experimental data in [37] are also listed in Table 5. Although the comparison with the experimental data is made in Table 5, it should be noted that there are some differences between methodologies. Kosma et al. have assigned their data to the

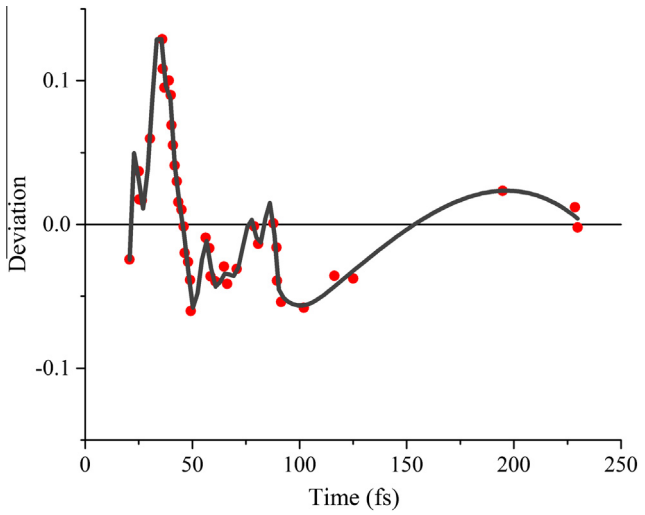

Fig. 9. Deviations of our simulation data from the $P(t)$ in the case of excitation to S_1.

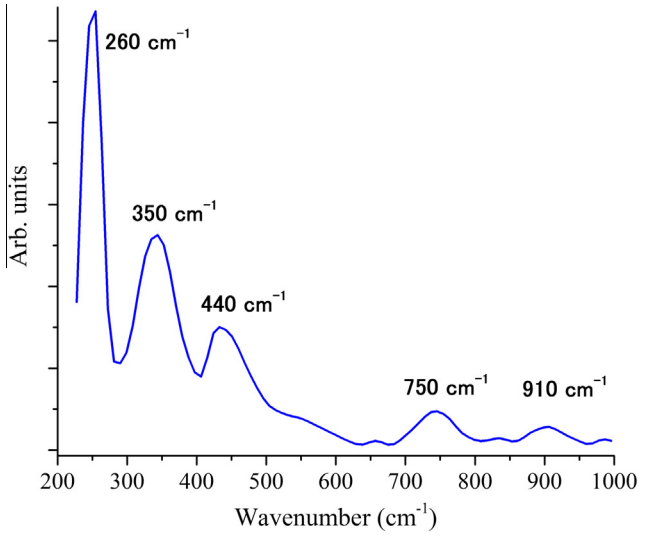

Fig. 10. Fourier transform of the deviations in the photoexcitation to S_1. Vertical axis shows the intensity of Fourier transformed data.

vibrational frequencies observed in S_0, while our frequency analysis was performed in S_1. Furthermore, the experimental data have been obtained by the laser excitation at 270 nm, but our simulation is based on the Franck–Condon principle, that is, the photoexcitation by the flash lamp. As shown in Table 5, the vibrational mode with 350 cm^{-1} is the ring puckering mode (out-of-plane vibration), and this vibrational mode has broken a molecular symmetry. In addition, the oscillation with 910 cm^{-1} is the C—C stretching vibration. These motions obviously lead to a bond breaking and a structural change. These major vibrational modes agree well with experimental data. The minor distinctions appear at some of vibrational assignments because of the difference in the used methodology that is by laser or white-light excitation, but it could be concluded that major molecular frequencies dominating the dynamics were similarly appeared in the individual observations.

Time-profile of the fraction of trajectories in S_2 by the excitation to S_2 was shown in Fig. 11, the total lifetime of S_2 ($t_{S_2,total}$) was also determined by the same method used in the case of the photoexcitation to S_1. The fitted $P(t)$ and sample points are depicted as the blue line and red points, respectively. $t_{S_2,total}$ was found to be 23 fs by two constants; t_{lat} and t_{dec} listed in Table 4. It was revealed that the molecular dynamics in PES of S_2 is an ultrafast decaying process. Fig. 12 indicates temporal changes of two excited states (S_2 and S_1) and ground state (S_0). The fraction of trajectories in S_2 was reduced immediately after the photoexcitation, while that of S_1 was quickly raised. The fraction of trajectories in S_1 peaked at t = 30 fs, and then trajectories going in and out of S_1 were observed in the figure; the first decay appeared around 40 fs just after the first peak, the second subsidiary peak appeared around 75 fs with the second decay, and the last decay around 125 fs was slower than the first two decays. This stepwise relaxation was explained as resulting from the existence of trajectories that failed to pass through the CoIn on their first attempt. When the trajectories reached around the CoIn, a portion of the trajectories passed through the CoIn and decayed to the S_0 PES. On the other hand, the remaining trajectories on the PES of S_1 continued to travel on the same PES until the next opportunity of decaying to S_0. Therefore, the number of relaxation-processes is regarded as the number of trying to decay. Focusing on Fig. 12 again, the decaying process of S_2 (that is, the increasing process of the fraction of trajectories in S_1) has two-stage process. Whereas all trajectories were proceeding from Franck–Condon region toward CoIn after photoexcitation to S_2, this stepwise relaxation was observed. As will be discussed in the next subsection, the molecular structures when nonadiabatic transition could happen were implicitly confined to a certain geometry shown in Fig. 17. Most of trajectories passed through the almost same CoIn of S_2, and this stepwise relaxation in the decaying process in S_2 is assumed as the result of transition-failure to S_1 at the CoIn geometry.

3.3. Branching ratio and nonadiabatic coupling vectors

Each trajectory was propagated over 600 fs after decay to S_0 to determine the product branching ratio (CHD:HT). As shown in Fig. 7, HT includes cZt-HT and tZt-HT. The branching ratio after

Table 5
The assignment of the frequencies given by FFT, the frequency analysis in S_1 and the experimental assignment.

The present work			Experimental data	
Vibrational level			Vibrational level in Ref. [37]/cm^{-1}	Assignment in Ref. [37]
FFT[a]/cm^{-1}	Frequency analysis[b]/cm^{-1}	Theoretical assignment		
–	–	–	140	Vibration in the S_0/S_1 CoIn direction
260	–	–	270	Ring puckering
350	350	Ring puckering (out of plane)	310	Ring puckering
440	501	Whole ring bending	–	–
750	713	C2–C3–C4, C4–C5–C6 bending	630	Ring puckering
910	910	C1–C2, C3–C4 stretching	950	C—C stretching
–	1418	C—H wagging	1430	C=C stretching

[a] Given by FFT.
[b] Vibration frequency analysis in S_1.

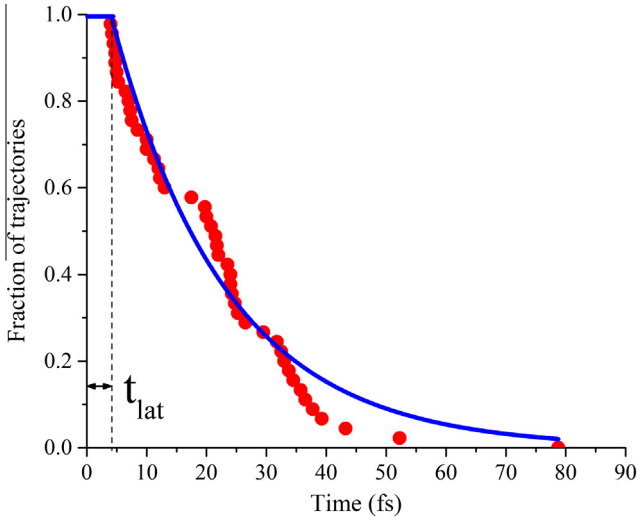

Fig. 11. Fraction of trajectories in S_2 after photoexcitation to S_2; red points were given by our simulations, while the blue line was the decay curve determined by Eq. (1.2). (For interpretation of the references to color in this figure legend, the reader is referred to the web version of this article.)

S_1 excitation was 60:40, where the HT product actually included these two structural isomers. This ratio also agrees with previous studies 50:50 or 60:40 [12,16,27]. The typical nonadiabatic coupling vector of nonadiabatic transition at CoIn of S_0/S_1 is shown in Fig. 13, which was quite similar to a Kekulé-type vibration involving the ring C—C stretching motions like benzene. In the photoexcitation to S_1, this motion appeared in almost all the trajectories; these motions were predicted by the fast Fourier transform of the deviation for S_1 population (the fraction of trajectories in S_1) in the previous section.

The branching ratio after excitation to S_2 was found to be 70:30. This result is quite different from the case of excitation to S_1, which suggests a rather strong selectivity. Since there are no studies on the S_2 excitation, there is no available experimental data to compare with our simulations. The details about the cause of this strong selectivity will be discussed while also considering the locations of CoIns later. The typical C3–C4–C5 bending motion (see Fig. 14) was found at nonadiabatic transition by CoIn of S_1/S_2. The molecular symmetry was broken due to this transition from

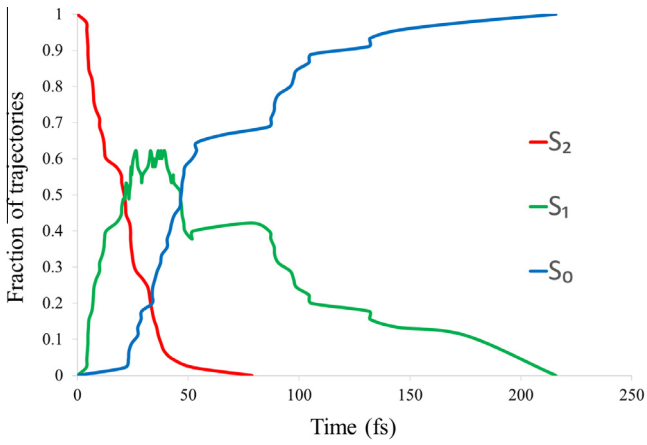

Fig. 12. The time-profile of fraction of trajectories in each states (S_2, S_1, and S_0) in the case of photoexcitation to S_2; red, green, and blue lines are the temporal change of fraction of trajectories in S_2, S_1 and S_0. (For interpretation of the references to color in this figure legend, the reader is referred to the web version of this article.)

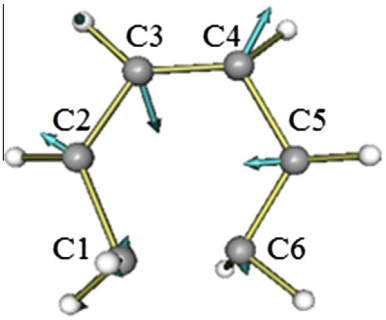

Fig. 14. Nonadiabatic coupling vector at S_2–S_1 CoIn; C3–C4–C5 bending motion.

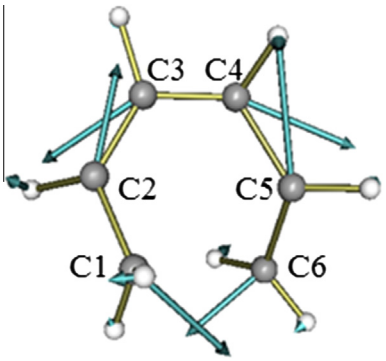

Fig. 13. Nonadiabatic coupling vector at S_1–S_0 CoIn; Kekulé-type vibration.

C_2 symmetry, but the molecular structure has still kept to be the ring structure of CHD. After that, the ring C—C stretching motions also appeared at nonadiabatic transition by CoIn of S_0/S_1, which is quite similar to the case of photoexcitation to S_1; the Kekulé-type vibration caused the second nonadiabatic transition at CoIn of S_0/S_1. The nonadiabatic transitions have happened with the strong relation to these two dynamical motions, which are not associated with the simple ring-opening motion as discussed in some previous studies.

Our simulations reveal that these two motions cause the nonadiabatic transition, but these motions alone have no direct relation to which products were generated because almost all trajectories showed same nonadiabatic coupling vectors. Fig. 15 displays the correlation map between the C1–C6 bond length and the C1–C3–C4–C6 dihedral angle (see Figs. 13 and 14) at the moment when the nonadiabatic transition happened for the case of photoexcitation to S_1. The triangle indicates the location of the equilibrium geometry of CHD. As a result, the coordinates produced CHD were scattered around the equilibrium CHD when the nonadiabatic transition occurred at CoIn of S_0/S_1, while the coordinates of produced HT show linearity between these two coordinates. Fig. 16 shows the same correlation map as Fig. 15 for transitions at CoIn of S_0/S_1 after photoexcitation to S_2. In the reaction pathway to produce HT, there is also linearity between the bond length and dihedral angle, which is reasonably described by the electronic structures of (22a) and (23a) MOs. The coordinates at nonadiabatic transitions by the CoIn of S_1/S_2 after photoexcitation to S_2 were also mapped in Fig. 17. These coordinates at the CoIn of S_1/S_2 were mainly located near the equilibrium geometry of CHD. This centered distribution results in the more one-sided branching ratio in S_2 excitation. The ratio of 70:30 was reported by Hofmann and de Vivie-Riedle [12]. They have investigated the effect of the difference between two CoIns ($CoIn_{min}$ and C_2-CoIn) on S_1 that dominated the CHD:HT ratio. In their discussion, the ratio of 70:30

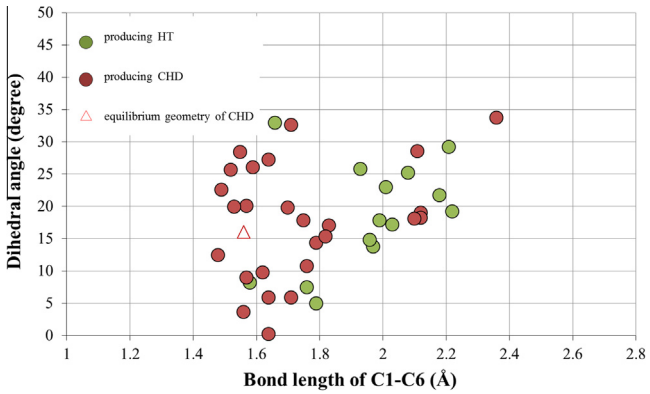

Fig. 15. Molecular coordinates passing through the CoIn of S_0/S_1 after excitation to S_1; red and green circles produced CHD and HT, respectively. (For interpretation of the references to color in this figure legend, the reader is referred to the web version of this article.)

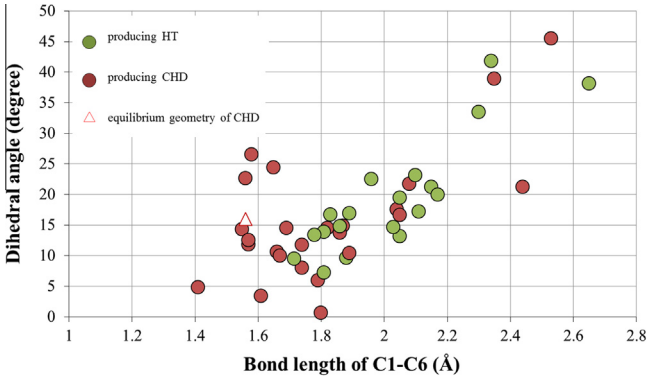

Fig. 16. Molecular coordinates passing through the CoIn of S_0/S_1 after excitation to S_2; red and green circles produced CHD and HT, respectively. (For interpretation of the references to color in this figure legend, the reader is referred to the web version of this article.)

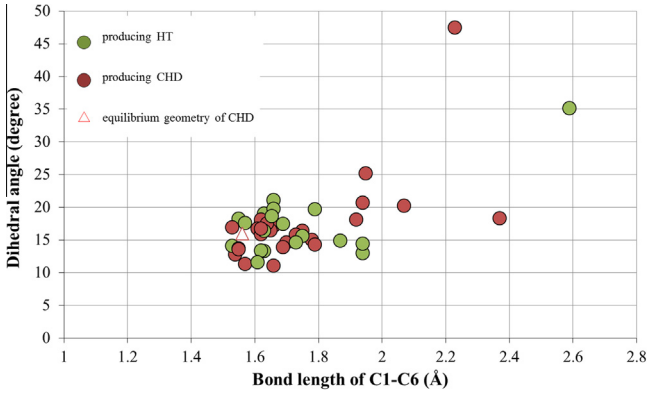

Fig. 17. Molecular coordinates passing through the CoIn of S_1/S_2 after excitation to S_2; red and green circles produced CHD and HT, respectively. (For interpretation of the references to color in this figure legend, the reader is referred to the web version of this article.)

were obtained by the case that all trajectories returned to S_0 with passing through the $CoIn_{min}$ on S_1 in the quantum wave packet propagation, and then the $CoIn_{min}$ were located near the CoIn of S_1/S_2. It is easy to expect that the trajectories decaying from S_2 have a tendency to pass the nearest CoIn. Our results about the excitation to S_2 resembled this situation. Since the molecule has the coordinates near the equilibrium geometry of CHD at the transition of CoIn of S_1/S_2, these coordinates are close to the region that produces CHD by CoIn of S_0/S_1. Thus, the 70:30 ratio is induced by the coordinates when the nonadiabatic transition occurs at CoIn of S_1/S_2; the nonadiabatic coupling vector at this CoIn features the simple bending motion and this bending motion didn't cause the large change of the initial molecular structure of CHD.

4. Conclusions

In the present work, the nonadiabatic *ab initio* molecular dynamics simulation based on trajectory surface-hopping approach was performed to find out the detailed dynamics of the photoisomerization between CHD and HT. The photoexcitation of CHD from zero-point vibration of S_0 was assumed without keeping a fixed the C_2 symmetry, so the photoexcitations to S_1 and S_2 were simulated with the full-dimensional model. CHD molecule was photoexcited and the number of time-evolved trajectories for each excitation to S_1 and S_2 were forty-two and forty-five, and then lifetimes of excited states and branching ratios (CHD:HT) were determined by statistical analysis.

Two excited states (S_2 and S_1) were located close to each other around Franck–Condon region. The energy fluctuation was the signature of the energy redistribution. In the case of S_1 excitation, the lifetime is 68 fs and is in agreement with literature data [10,16,30,37], while in photoexcitation to S_2, a short lifetime was observed (23 fs). The fast Fourier transform of the deviation for S_1 population revealed that several molecular vibrations on S_1, and the vibration with 350 and 910 cm^{-1} were the ring puckering mode (the out-of plane vibration) and the C—C stretching motion, respectively. These motions have played important roles for this reaction-mechanism. In the case of photoexcitation to S_2, time-profiles of fractions of trajectories in S_2 and S_1 have shown stepwise relaxations. Especially the decaying process of S_1 has three-stage relaxation. These stepwise relaxations were explained as resulting from the existence of trajectories that failed to pass through the fixed CoIn on their first attempt. When trajectories reached the CoIn, trajectories branched into two routes; the route is to pass through the CoIn to reach S_1, while the other is to stay in S_2. This branching process appeared as the stepwise process. In order to clarify molecular motions related to the nonadiabatic transition, the nonadiabatic coupling vector were explored at the molecular structure which has two states closed. The Kekulé-type vibration (like as the C—C bond stretching motion with 910 cm^{-1}) caused the nonadiabatic transition at CoIn of S_0/S_1 as some previous studies mentioned. On the other hand, it is important to occur the symmetry collapse with the C4–C5–C6 bending motion at CoIn of S_1/S_2. Nevertheless, the molecular coordinates were keeping CHD structure at this CoIn. These motions had been seen in almost trajectories at each simulation in both cases of the excitation to S_1 and S_2.

It turned out that the branching ratio is 60:40 by our simulation about the photoexcitation to S_1. This result compares well with the experimental data in solution (60:40) [27]. On the other hand, the branching ratio in the photoexcitation to S_2 results in the 70:30 ratio. Since almost trajectories had same nonadiabatic coupling vectors, the nonadiabatic vectors at each CoIns did not have no relation to the CHD:HT ratio. This characteristic ratio is governed by the centered distribution in the correlation map of C1–C6 bond length and dihedral angle at CoIn of S_1/S_2 around the region that mainly produces CHD on S_1. At CoIn of S_1/S_2, most of trajectories have taken the same molecular motions (bending motion) and still kept CHD structure as we discussed. Since any studies about the photoexcitation to S_2 on the photoisomerization between CHD and HT have not been investigated, we hope some experimental group would make sure of our perspective.

Conflict of interest

There is no conflict of interest.

Acknowledgments

The authors would like to thank Hiroki Nakamura (Department of Applied Chemistry, National Chiao Tung University, Taiwan) for his constructive comments and Shunsuke Adachi (Department of Chemistry, Kyoto University, Japan) for his experimental comments. A.O. is indebted to the Research Fellow of Japan Society for the Promotion of Science (DC1) and this study was supported by the Grant-in-Aid for JSPS Fellows (No. 26004667), a Grant-in-Aid for Scientific Research (S) (No. 23224013) and Grant-in-Aid for Scientific Research (A) (No. 26248038) from the Ministry of Education, Culture, Sports, Science and Technology (MEXT), Japan.

References

[1] M. Irie, Chem. Rev. 100 (2000) 2000, http://dx.doi.org/10.1021/cr980069d.
[2] M. Irie, S. Kobatake, M. Horichi, Science 291 (2001) 1769, http://dx.doi.org/10.1126/science.291.5509.1769.
[3] M. Murakami, H. Miyasaka, T. Okada, S. Kobatake, M. Irie, J. Am. Chem. Soc. 126 (2004) 14764, http://dx.doi.org/10.1021/ja049177+.
[4] K.L. Kompa, R.D. Levine, Proc. Natl. Acad. Sci. U.S.A. (2001), http://dx.doi.org/10.1073/pnas.98.2.410.
[5] P. Celani, S. Ottani, M. Olivucci, F. Bernardi, M.A. Robb, J. Am. Chem. Soc. 116 (1994) 10141, http://dx.doi.org/10.1021/ja00101a037.
[6] P. Celani, F. Bernardi, M.A. Robb, M. Olivucci, J. Phys. Chem. 100 (1996) 19364, http://dx.doi.org/10.1021/jp962206l.
[7] M. Garavelli, P. Celani, M. Fato, M.J. Bearpark, B.R. Smith, M. Olivucci, M.A. Robb, J. Phys. Chem. A 101 (1997) 2023, http://dx.doi.org/10.1021/jp961554k.
[8] M. Garavelli, P. Celani, F. Bernardi, M.A. Robb, M. Olivucci, J. Am. Chem. Soc. 119 (1997) 11487, http://dx.doi.org/10.1021/ja971280u.
[9] M. Garavelli, F. Bernardi, M. Olivucci, T. Vreven, S. Klein, P. Celani, M.A. Robb, Faraday Discuss. 110 (1998) 51, http://dx.doi.org/10.1039/a802270d.
[10] M. Garavelli, C.S. Page, P. Celani, M. Olivucci, W.E. Schmid, S.A. Trushin, W. Fuss, J. Phys. Chem. A 105 (2001) 4458, http://dx.doi.org/10.1021/jp010359p.
[11] A. Hofmann, R. de Vivie-Riedle, J. Chem. Phys. 112 (2000) 5054, http://dx.doi.org/10.1063/1.481059.
[12] A. Hofmann, R. De Vivie-Riedle, Chem. Phys. Lett. 346 (2001) 299, http://dx.doi.org/10.1016/S0009-2614(01)00922-8.
[13] L. Kurtz, A. Hofmann, R. de Vivie-Riedle, J. Chem. Phys. 114 (2001) 6151, http://dx.doi.org/10.1063/1.1355658.
[14] A. Hofmann, L. Kurtz, R. de Vivie-Riedle, Appl. Phys. B 71 (2000) 391, http://dx.doi.org/10.1007/s003400000355.
[15] H. Tamura, S. Nanbu, H. Nakamura, T. Ishida, Chem. Phys. Lett. 401 (2005) 487, http://dx.doi.org/10.1016/j.cplett.2004.11.111.
[16] H. Tamura, S. Nanbu, T. Ishida, H. Nakamura, J. Chem. Phys. 124 (2006) 084313, http://dx.doi.org/10.1063/1.2171688.
[17] C. Nonnenberg, S. Grimm, I. Frank, J. Chem. Phys. 119 (2003) 11585, http://dx.doi.org/10.1063/1.1623743.
[18] M. Boggio-Pasqua, M. Ravaglia, M.J. Bearpark, M. Garavelli, M.A. Robb, J. Phys. Chem. A 107 (2003) 11139, http://dx.doi.org/10.1021/jp036862e.
[19] J.B. Schönborn, J. Sielk, B. Hartke, J. Phys. Chem. A 114 (2010) 4036, http://dx.doi.org/10.1021/jp909362c.
[20] M.O. Trulson, G.D. Dollinger, R.A. Mathies, Femtosecond photochemical ring opening dynamics of 1,3-cyclohexadiene from resonance raman intensities, J. Am. Chem. Soc. 109 (1987) 586, http://dx.doi.org/10.1021/ja00236a049.
[21] M.O. Trulson, G.D. Dollinger, R.A. Mathies, J. Chem. Phys. 90 (1989) 4274, http://dx.doi.org/10.1063/1.455784.
[22] P.J. Reid, S.J. Doig, R.A. Mathies, Chem. Phys. Lett. 156 (1989) 163, http://dx.doi.org/10.1016/S0009-2614(89)87113-1.
[23] P.J. Reid, S.D. Wickham, R.A. Mathies, J. Phys. Chem. 96 (1992) 5720, http://dx.doi.org/10.1021/j100193a013.
[24] P.J. Reid, S.J. Doig, S.D. Wickham, R.A. Mathies, J. Am. Chem. Soc. 115 (1993) 4754, http://dx.doi.org/10.1021/ja00064a040.
[25] M.K. Lawless, S.D. Wickham, R.A. Mathies, Acc. Chem. Res. 28 (1995) 493, http://dx.doi.org/10.1021/ar00060a005.
[26] S. Pullen, L.A. Walker II, B. Donovan, R.J. Sension, Chem. Phys. Lett. 242 (1995) 415, http://dx.doi.org/10.1016/0009-2614(95)00772-V.
[27] S.H. Pullen, N.A. Anderson, L.A. Walker II, R.J. Sension, J. Chem. Phys. 108 (1998) 556, http://dx.doi.org/10.1063/1.476366.
[28] S. Lochbrunner, W. Fuss, W.E. Schmid, K.L. Kompa, J. Phys. Chem. A 102 (1998) 9334, http://dx.doi.org/10.1021/jp9809179.
[29] W. Fuß, T. Schikarski, W.E. Schmid, S. Trushin, K.L. Kompa, Chem. Phys. Lett. 262 (1996) 675, http://dx.doi.org/10.1016/S0009-2614(96)01149-9.
[30] S.A. Trushin, W. Fuss, T. Schikarski, W.E. Schmid, K.L. Kompa, J. Chem. Phys. 106 (1997) 9386, http://dx.doi.org/10.1063/1.474009.
[31] W. Fuß, W.E. Schmid, S.A. Trushin, J. Chem. Phys. 112 (2000) 8347, http://dx.doi.org/10.1063/1.481478.
[32] N. Kuthirummal, F.M. Rudakov, C.L. Evans, P.M. Weber, J. Chem. Phys. 125 (2006) 133307, http://dx.doi.org/10.1063/1.2345203.
[33] R.C. Dudek, P.M. Weber, J. Phys. Chem. A 105 (2001) 4167, http://dx.doi.org/10.1021/jp010122t.
[34] J.D. Cardoza, R.C. Dudek, R.J. Mawhorter, P.M. Weber, Chem. Phys. 299 (2004) 307, http://dx.doi.org/10.1016/j.chemphys.2003.12.018.
[35] C.Y. Ruan, V.A. Lobastov, R. Srinivasan, B.M. Goodson, H. Ihee, A.H. Zewail, Proc. Natl. Acad. Sci. U.S.A. 98 (2001) 7117, http://dx.doi.org/10.1073/pnas.131192898.
[36] H. Ihee, V.A. Lobastov, U.M. Gomez, B.M. Goodson, R. Srinivasan, C.Y. Ruan, A.H. Zewail, Science (2001), http://dx.doi.org/10.1126/science.291.5503.458.
[37] K. Kosma, S.A. Trushin, W. Fuss, W.E. Schmid, Phys. Chem. Chem. Phys. 11 (2009) 172, http://dx.doi.org/10.1039/b814201g.
[38] S. Adachi, M. Sato, T. Suzuki, J. Phys. Chem. Lett. 6 (2015) 343, http://dx.doi.org/10.1021/jz502487r.
[39] M.P. Minitti, J.M. Budarz, A. Kirrander, J.S. Robinson, D. Ratner, T.J. Lane, D. Zhu, J.M. Glownia, M. Kozina, H.T. Lemke, M. Sikorski, Y. Feng, S. Nelson, K. Saita, B. Stankus, T. Northey, J.B. Hastings, P.M. Weber, Phys. Rev. Lett. 114 (2015) 255501, http://dx.doi.org/10.1103/PhysRevLett. 114.255501.
[40] S.O. Danielache, M.S. Johnson, S. Nanbu, M.M.L. Grage, C. McLinden, N. Yoshida, Chem. Phys. Lett. 450 (2008) 214, http://dx.doi.org/10.1016/j.cplett.2007.11.054.
[41] J.A. Schmidt, M.S. Johnson, S. Hattori, N. Yoshida, S. Nanbu, R. Schinke, Atmos. Chem. Phys. 13 (2013) 1511, http://dx.doi.org/10.5194/acp-13-1511-2013.
[42] J.C. Tully, R.K. Preston, J. Chem. Phys. 55 (1971) 562, http://dx.doi.org/10.1063/1.1675788.
[43] J.C. Tully, J. Chem. Phys. 07974 (1990) 1061, http://dx.doi.org/10.1063/1.459170.
[44] S. Nanbu, T. Ishida, H. Nakamura, Chem. Sci. 1 (2010) 663, http://dx.doi.org/10.1039/c0sc00274g.
[45] C. Zhu, K. Nobusada, H. Nakamura, J. Chem. Phys. 115 (2001) 3031, http://dx.doi.org/10.1063/1.1386811.
[46] C. Zhu, H. Kamisaka, H. Nakamura, J. Chem. Phys. 115 (2001) 11036, http://dx.doi.org/10.1063/1.1421070.
[47] C. Zhu, H. Kamisaka, H. Nakamura, J. Chem. Phys. 116 (2002) 3234, http://dx.doi.org/10.1063/1.1446032.
[48] P. Oloyede, G. Mil'nikov, H. Nakamura, J. Chem. Phys. 124 (2006) 144110, http://dx.doi.org/10.1063/1.2187978.
[49] H. Nakamura, J. Phys. Chem. A 110 (2006) 10929, http://dx.doi.org/10.1021/jp063643v.
[50] C. Zhu, H. Nakamura, N. Re, V. Aquilanti, J. Chem. Phys. 97 (1992) 1892, http://dx.doi.org/10.1063/1.463178.
[51] C. Zhu, H. Nakamura, J. Chem. Phys. 97 (1992) 8497, http://dx.doi.org/10.1063/1.463368.
[52] C. Zhu, H. Nakamura, J. Chem. Phys. 98 (1993) 6208, http://dx.doi.org/10.1063/1.464814.
[53] C. Zhu, H. Nakamura, J. Chem. Phys. 101 (1994) 4855, http://dx.doi.org/10.1063/1.468505.
[54] C. Zhu, H. Nakamura, J. Chem. Phys. 101 (1994) 10630, http://dx.doi.org/10.1063/1.467877.
[55] C. Zhu, H. Nakamura, J. Chem. Phys. 102 (1995) 7448, http://dx.doi.org/10.1063/1.469057.
[56] C. Zhu, H. Nakamura, J. Chem. Phys. 106 (1997) 2599, http://dx.doi.org/10.1063/1.473364.
[57] C. Zhu, H. Nakamura, J. Chem. Phys. 107 (1997) 7839, http://dx.doi.org/10.1063/1.475096.
[58] C. Zhu, H. Nakamura, J. Chem. Phys. 108 (1998) 7501, http://dx.doi.org/10.1063/1.476321.
[59] Nonadiabatic Transition: Concepts, Basic Theories and Applications, World Scientific Publishing Co Pte Ltd.
[60] N. Shenvi, J.E. Subotnik, W. Yang, J. Chem. Phys. 134 (2011) 144102, http://dx.doi.org/10.1063/1.3575588.
[61] N. Shenvi, J.E. Subotnik, W. Yang, J. Chem. Phys. 135 (2011) 024101, http://dx.doi.org/10.1063/1.3603447.
[62] T.H. Dunning, J. Chem. Phys. 90 (1989) 1007, http://dx.doi.org/10.1063/1.456153.
[63] C. Xie, X. Hu, L. Zhou, D. Xie, H. Guo, J. Chem. Phys. 139 (2013) 014305, http://dx.doi.org/10.1063/1.4811840.
[64] W.C. Swope, H.C. Andersen, P.H. Berens, K.R. Wilson, J. Chem. Phys. 76 (1982) 637, http://dx.doi.org/10.1063/1.442716.
[65] E. Wigner, Phys. Rev. (1932), http://dx.doi.org/10.1103/PhysRev. 40.749.
[66] T. Ishida, S. Nanbu, H. Nakamura, J. Phys. Chem. A 113 (2009) 4356, http://dx.doi.org/10.1021/jp8110315.
[67] W.C. Chung, S. Nanbu, T. Ishida, J. Phys. Chem. A 114 (2010) 8190, http://dx.doi.org/10.1021/jp103253b.
[68] T. Murakami, M. Nakazono, A. Kondorskiy, T. Ishida, S. Nanbu, Phys. Chem. Chem. Phys. 14 (2012) 11546, http://dx.doi.org/10.1039/c2cp41269a.
[69] W.C. Chung, S. Nanbu, T. Ishida, J. Phys. Chem. B (2012), http://dx.doi.org/10.1021/jp212378u.
[70] S. Gozem, M. Huntress, I. Schapiro, R. Lindh, A.A. Granovsky, C. Angeli, M. Olivucci, J. Chem. Theory Comput. 8 (2012) 4069, http://dx.doi.org/10.1021/ct3003139.
[71] S.O. Danielache, S. Nanbu, C. Eskebjerg, M.S. Johnson, N. Yoshida, J. Chem. Phys. 131 (2009), http://dx.doi.org/10.1063/1.3156314.
[72] S. Nanbu, M.S. Johnson, J. Phys. Chem. A 108 (2004) 8905, http://dx.doi.org/10.1021/jp048853r.